

See discussions, stats, and author profiles for this publication at: <https://www.researchgate.net/publication/277961573>

Synthesis and characterization of graphitic mesoporous carbon using metal–metal oxide by chemical vapor deposition method

ARTICLE in MICROPOROUS AND MESOPOROUS MATERIALS · MAY 2015

Impact Factor: 3.45 · DOI: 10.1016/j.micromeso.2015.05.032

CITATIONS

4

READS

41

5 AUTHORS, INCLUDING:



R. Atchudan

Yeungnam University

17 PUBLICATIONS 123 CITATIONS

[SEE PROFILE](#)

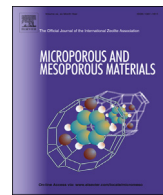


Pandurangan Arumugam

Anna University, Chennai

155 PUBLICATIONS 1,881 CITATIONS

[SEE PROFILE](#)



Synthesis and characterization of graphitic mesoporous carbon using metal–metal oxide by chemical vapor deposition method

Raji Atchudan ^{a, c, *}, Suguna Perumal ^b, Dhanapalan Karthikeyan ^d, Arumugam Pandurangan ^c, Yong Rok Lee ^{a, **}

^a School of Chemical Engineering, Yeungnam University, Gyeongsan 712-749, Republic of Korea

^b Department of Applied Chemistry, Kyungpook National University, Daegu 702-701, Republic of Korea

^c Department of Chemistry, CEG Campus, Anna University, Chennai 600025, India

^d Arignar Anna College of Arts and Science, Krishnagiri 635001, Tamil Nadu, India



ARTICLE INFO

Article history:

Received 31 March 2015

Received in revised form

14 May 2015

Accepted 15 May 2015

Available online 27 May 2015

Keywords:

Catalytic template

Magnesium oxide

Acetylene

Graphitic mesoporous carbon

Chemical vapor deposition

ABSTRACT

Mn/MgO was prepared by wet impregnation method and was used as a catalytic template for the growth of graphitic mesoporous carbon (GMC) using acetylene gas as carbon precursor at 900 °C by CVD method. The deposited carbon nanostructured material was separated from the catalytic template by the acid treatment, and was investigated by various physico-chemical techniques such as XRD, BET, SEM, TEM, and Raman spectroscopy. The BET surface area of GMC is ca. 200 m² g⁻¹. The XRD pattern and Raman spectroscopic techniques revealed the crystallinity and the degree of graphitization of mesoporous carbon. The interlayer distance of graphene sheet in GMC is around 0.34 nm. All the analytical results strongly support that the prepared mesoporous carbon to be highly ordered and well in graphitic nature. Further, the results demonstrate that the GMC synthesized by using a Mn/MgO might be a promising contender for the large-scale synthesis.

© 2015 Elsevier Inc. All rights reserved.

1. Introduction

Porous carbon has attracted increasing attention due to its potential applications as large molecular adsorbent, catalyst support, fuel cells, electrode materials for supercapacitors and lithium batteries, etc. [1–11]. Various conventional synthesis methods, including arc discharge, laser evaporation, and chemical vapor deposition, have used to prepare graphitic carbons. The synthesis of graphitic mesoporous carbon (GMC) by the CVD has attracted much attention due to many advantages such as high purity, low cost, moderate temperature used for the production, and scalable technique for mass production compared to other methods [12–14]. The catalytically produced GMC is adequate for many applications, especially in mechanical, electronic devices and active catalytic support for fine chemical synthesis because they can be directly

synthesized without major contamination by carbonaceous impurities. Different types of mesoporous silica materials has been used as a catalytic template for the production of GMC with sucrose, glucose, citrate compound, propylene, resorcinol, formaldehyde, xylene, poly-vinyl compound and etc. as carbon precursor [15–17]. In these cases, the removal of silica from the mesoporous carbon is difficult. So we have to use strong hydrofluoric acid for the purification process and during this process the ordered structure of GMC is damaged.

In the present work, we have synthesized mesoporous carbon with high graphitization using Mn loaded MgO as a catalytic template and acetylene as carbon precursor by an economical method. Here MgO (Light) was used as a catalytic template instead of other catalytic templates such as silica based porous materials and porous metal oxides because it is easily available and economy. MgO is a versatile material widely used in nano-community as a catalytic template for the production of carbon nanostructure and as catalyst for the production of fine chemicals. Carbon rich acetylene is as a precursor for the production of GMC and the dilute aqua regia was used for the purification of GMC. The results showed that the GMC synthesized from acetylene over the Mn/MgO catalytic template have higher degree of graphitization.

* Corresponding author. School of Chemical Engineering, Yeungnam University, Gyeongsan 712-749, Republic of Korea. Tel.: +82 53 810 3566; fax: +82 53 810 4631.

** Corresponding author. Tel.: +82 53 810 2529; fax: +82 53 810 4631.

E-mail addresses: atchudan@yahoo.com (R. Atchudan), [\(Y.R. Lee\).](mailto:yrllee@yu.ac.kr)

2. Experimental

2.1. Materials

Manganese acetate, Magnesium oxide (Light), hydrochloric acid and nitric acid were purchased from Merck Chemical Ltd and were used as received without any further purification. Acetylene gas (>99%), hydrogen gas (>99%) and nitrogen gas (>99%) were used for the production of mesoporous carbon. The double distilled (DD) water was used throughout this study.

2.2. Preparation of Mn/MgO

Different amounts of Mn (Mn: 5, 10 and 15 wt%) were loaded over the MgO (Light) using the wet impregnation method [18]. In a typical procedure, the appropriate amount of manganese acetate solution was prepared through sonication process and then mixed with MgO under constant stirring. The solution was dried under reduced pressure and then calcined in a muffle furnace at 600 °C for 5 h under static condition. The furnace was cooled to room temperature and then final impregnated material was collected and stored for use.

2.3. Synthesis and purification of GMC

The catalytic reactions for the synthesis of GMC were carried over the calcined Mn/MgO catalytic template using acetylene by CVD under atmospheric pressure. The experiment was carried out in a simple CVD setup containing horizontal tubular furnace and gas flow control units and the schematic illustration is shown in Fig. 1. In a typical growth experiment, ca.200 mg catalytic template was placed in a quartz boat inside a quartz tube. The catalytic template was purged by nitrogen gas at a flow rate of 500 mL/min for 30 min to remove the physically adsorbed water molecules. Then the catalytic template was purged using hydrogen gas at a flow rate of 100 mL/min for 30 min to reduce the metal oxide nanoparticles. The reaction was carried out using acetylene as a carbon precursor at 900 °C with flow rate of 100 mL/min for 30 min. The furnace was allowed to cool under nitrogen atmosphere and the final product was weighed and purified. The similar reaction was carried out at different temperatures (800 and 1000 °C). The percentage of the carbon deposition (CD) due to the catalytic

decomposition of acetylene was calculated from the following equation (1):

$$\text{Yield of CD}(\%) = \frac{M_{\text{tot}} - M_{\text{cat}}}{M_{\text{cat}}} \times 100 \quad (1)$$

where, M_{tot} and M_{cat} are the total mass of carbon product with catalytic template and mass of catalytic template, respectively.

The metal/metal oxide was removed by treating with mixture of hydrochloric acid and nitric acid at ambient temperature, as found in literature [19]. In a typical procedure, as-synthesized carbon sample was immersed with an appropriate amount of dilute mixture of hydrochloric acid and nitric acid. The final mixture was filtered to remove the metal particles from GMC and followed by the solid sample was washed with DD water until solution reaches to pH 7. The filtered material was dried at 100 °C for 5 h in a hot air oven [20,21] and was calcined at 350 °C for 2 h in a muffle furnace under static condition. The furnace was then cooled to room temperature and the pure GMC was collected and characterized.

2.4. Characterization methods

The synthesized Mn/MgO and GMC were characterized by various physico-chemical techniques such as X-ray diffraction (XRD), Nitrogen physisorption studies, scanning electron microscopy (SEM), transmittance electron microscopy (TEM) and Raman spectroscopy. The XRD patterns of the Mn/MgO and GMC were obtained with a PANalytical X'Pert using nickel-filtered Cu K α as the radiation source ($\lambda = 1.54 \text{ \AA}$) and a liquid nitrogen cooled germanium based solid-state device as the detector. The XRD patterns of the materials were recorded in the scattering angle 2θ range of 5–80°, at a step interval of 0.02° and an integration time of 5 s at each step. Nitrogen adsorption-desorption isotherms were measured at –197 °C using a Micromeritics ASAP 2000. Prior to the experiments, the samples were dried at 130 °C and evacuated for 8 h in flowing argon at the flow rate of 60 SCCM at 150 °C. Surface area, pore size, and pore volumes were obtained from isotherms using the conventional Brunauer–Emmet–Teller (BET) and Barrett–Joyner–Halenda (BJH) equations. SEM analysis was performed on a JEOL with acceleration voltage of 4 kV. Sample was sonicated with ethanol and placing on silicon wafer. TEM images of typical samples of GMC were obtained using a JEOL 3010 electron

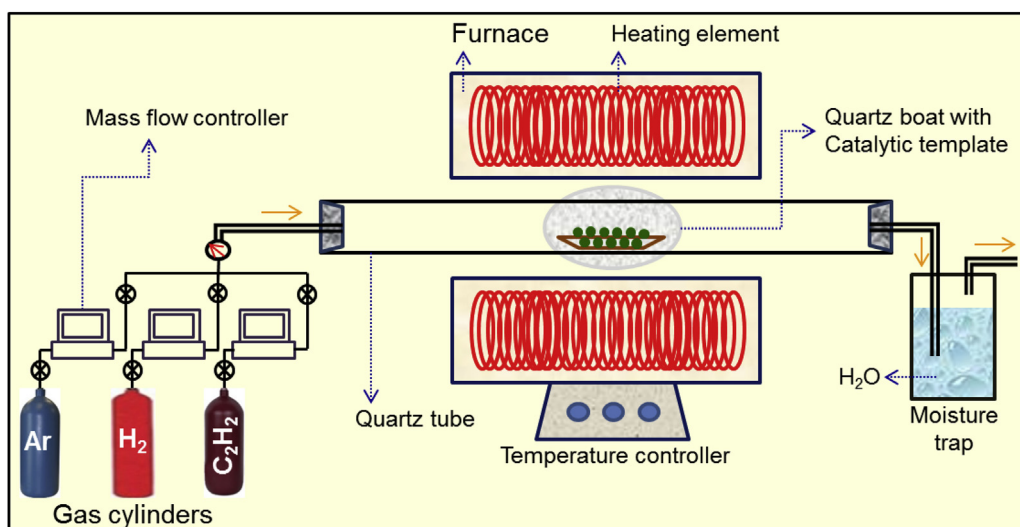


Fig. 1. Schematic illustration of CVD setup for the production of GMC.

microscope operated at 300 kV. Samples for TEM were prepared by placing droplets of a suspension of the sample in acetone on a polymer micro grid supported on a Cu grid. Raman spectra were recorded using Micro-Raman system RM 1000 Renishaw with a laser excitation line at 532 nm (Nd-YAG), 0.5–1 mW, with 1 μm focus spot in order to avoid photodecomposition of the samples.

3. Results and discussion

3.1. X-ray diffraction pattern of MgO and Mn/MgO

XRD analysis can provide information on the structural characteristics of material which includes crystallinity, phase and purity of the materials and also it gives average crystallite size of the material. The high-angle XRD patterns of MgO (light) and prepared 10 wt% Mn/MgO are shown in Fig. 2. The samples exhibit the reflections corresponding to cubic MgO phase [22]. The diffraction peaks of Mn impregnated MgO shift slightly towards to higher 2 theta values and the slightly broadening of diffraction lines is clearly seen in Fig. 2. This might be due to loading effect of Mn nanoparticles over the MgO light material. Absence of other impurity peaks confirms the formed material is highly pure with perfect crystalline structure.

3.2. X-ray diffraction pattern of GMC

High-angle XRD pattern of GMC obtained over the different wt% of Mn/MgO is shown in Fig. 3. The spectrum displays a strong peak around $2\theta = 26^\circ$ and weak peak around $2\theta = 43, 53^\circ$ which are assigned to C(002) and C(100), C(004) diffraction patterns of typical graphite, respectively [23,24]. The interlayer distance (d_{002}) calculated by Bragg's equation ($d = n\lambda/2\sin\theta$, where d is the spacing between the planes in the atomic lattice, n is an integer (1), λ is the wavelength of incident wave (1.54 Å), and θ is the angle between the incident ray and the scattering planes) based on the C(002) diffraction peak in Fig. 3. The interlayer distance (d_{002}) for Fig. 3(a), (b) and (c) is 0.346, 0.344 and 0.342 nm, respectively. There is no much more difference in the interlayer distance for the samples prepared from different weight percentage of Mn on MgO template. The interlayer distance of GMC is slightly decreasing with increase in metal concentration over the support, which is due to increasing hindrance with increasing the metal concentration in the specific area. The intensity of XRD peaks for GMC is first increased then

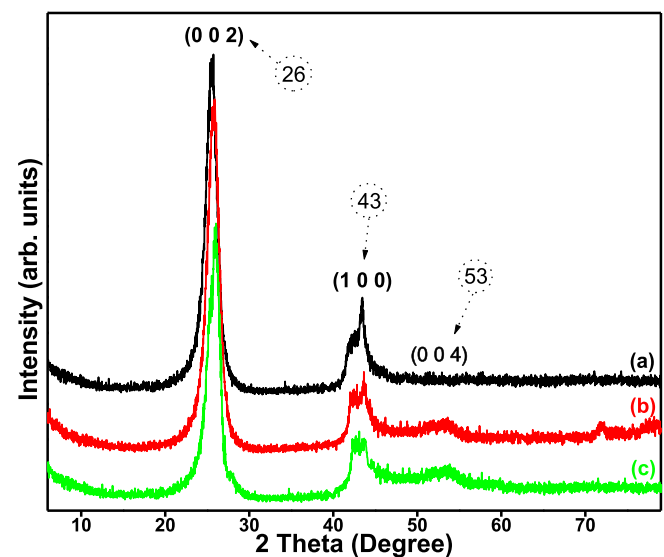


Fig. 3. XRD pattern of GMC obtained over the (a) 5 wt% Mn/MgO (b) 10 wt% Mn/MgO and (c) 15 wt% Mn/MgO at 900 °C.

decreased with increasing the metal concentration of nanoparticle (Mn) on the metal oxide support (MgO). The optimum for the better graphitization of GMC is obtained over the 10 wt% of Mn on MgO. The intensity of GMC obtained from 5 wt% Mn/MgO and 15 wt % Mn/MgO is little low because the insufficient amount of Mn present over the MgO to grow the GMC and insufficient amount of space to grow the GMC over the MgO, respectively. The pure GMC without major contaminations was confirmed by the absence of catalytic template and also the other impurity peaks in XRD pattern. The results strongly suggest that the formed GMC is well graphitized [25,26].

3.3. Nitrogen sorption studies of GMC

It is necessary to know the surface area and the pore size distribution from the nitrogen physisorption measurement. The physisorption curves of synthesized GMC are shown in Fig. 4 that indicate the presence of mesopores with a continuous size distribution. It contains a sharp capillary condensation step at high relative pressures ($P/P_0 > 0.9$) and an H3-type hysteresis loop, indicating the existence of large pores in the material [27,28]. In general, initial vertical part of the curve at low P/P_0 reveals the presence of micropores but in this isotherms are minor point of vertical part in low P/P_0 for all the samples. The obtained materials show trace micropores and major mesoporous in nature. The pore diameter gradually increases with increasing the Mn concentrations on the support and is clear with pore size distribution graph (Fig. 4). The surface area is nearly close for the GMC obtained over 5 wt% Mn/MgO and 10 wt% Mn/MgO. The surface area of GMC obtained from 5 wt% Mn/MgO is higher than GMC obtained from 15 wt% Mn/MgO. The adequate space is available for GMC growth over the 5 wt% Mn/MgO, after removing metals particle larger surface area was obtained. The surface area of GMC obtained over the 15 wt% Mn/MgO is lower than others because it is having sufficient amount of metal particle to grow the graphitic carbon but insufficient space over the MgO catalytic templates in specific area and thus lead to shrunk mesoporous carbon. GMC obtained over the 10 wt% Mn/MgO has high surface area and also high degree of graphitization. This GMC was calcined and studied for the N_2 physisorption properties. After calcination, the surface area

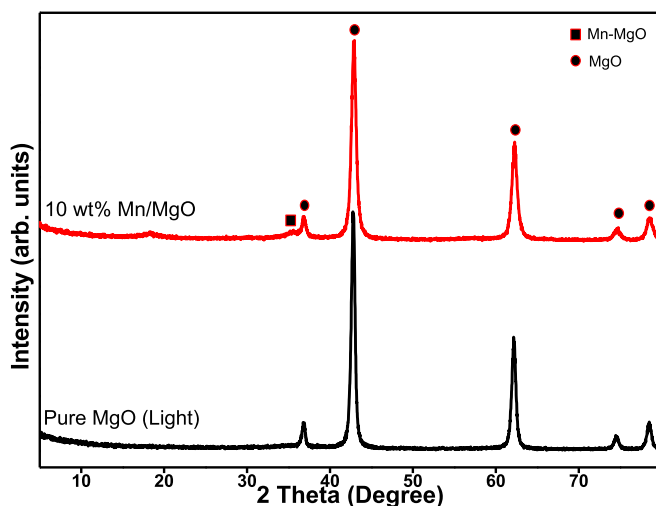


Fig. 2. The XRD pattern of MgO and prepared 10 wt% Mn/MgO catalytic template.

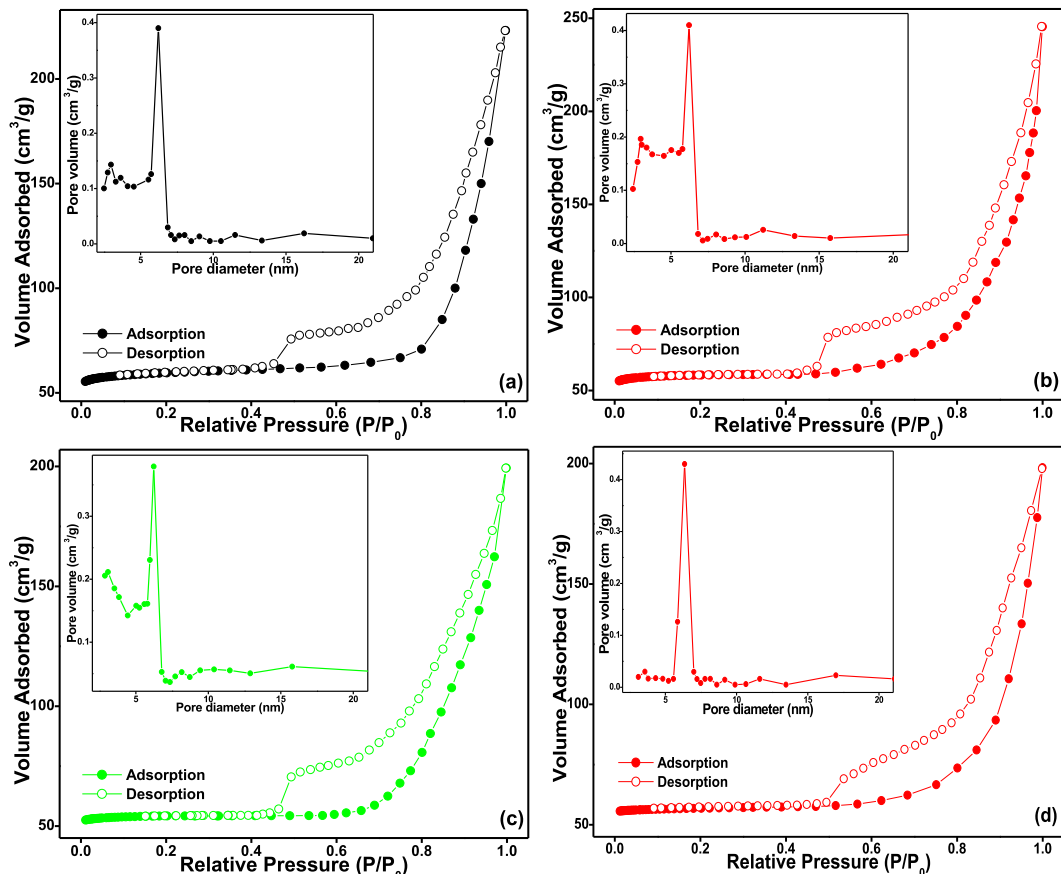


Fig. 4. Nitrogen physisorption isotherms and corresponding pore size distributions of GMC obtained over the (a) 5 wt% Mn/MgO (b) 10 wt% Mn/MgO and (c) 15 wt% Mn/MgO at 900 °C; (d) Nitrogen physisorption isotherms and corresponding pore size distributions of GMC (after calcination) obtained over the 10 wt% Mn/MgO.

decreased and pore diameter increased due to amorphous carbon and also low degree of graphitic carbon escaped from the GMC cage during the calcination. Generally, while increasing the graphitization, surface area will decrease but the obtained GMC has high surface area with well graphitization. The BJH pore size distribution of the GMC, and the BET surface areas, pore diameter and the pore volumes of the samples are summarized in Table 1.

3.4. SEM and TEM studies of GMC

The surface morphology of the nanomaterials and quantitative measurement of component was identified by using SEM along with energy-dispersive X-ray spectroscopy (EDS) technique. SEM images of as-synthesized GMC over the different wt% of Mn/MgO at 900 °C are shown in Fig. 5. The spongy like GMC was distributed uniformly throughout the matrix [29]. Large amount of carbon foams are formed over the Mn/MgO catalytic templates and clear from SEM images. The morphology varied slightly depending on

Mn concentration over the MgO support. The surface smoothness of formed materials is slightly decreasing with increase the Mn concentration of MgO support. The carbon deposition is on the surface of Mn nanoparticles over the MgO support. Larger cloudy carbon material is deposited on lower concentration of Mn over the MgO support. While increasing the metal concentration over the MgO support, smaller cloudy carbon materials obtained over the catalytic support due to insufficient face. The yield of CD increases with increasing the Mn concentration and then decreased which was confirmed by gravimetric calculation (eq. (1)). The Mn nanoparticles are seeds for the growth of carbon materials. The percentage yield of GMC is summarized in Table 2. Fig. 6 shows SEM images of GMC with different magnification after removal of catalytic templates. SEM images clearly show that more smooth and spongy morphological GMC is obtained after acid treatment because the catalytic template is eliminated from the deposited carbon materials. After elimination of the metal particles holes (porous) are formed on the deposited carbon. SEM with EDS images

Table 1

Textural properties of the GMC obtained over the different catalytic templates at 900 °C.

S. No	Synthesized material	Catalytic template	d-Spacing value (Å) ^a	Surface area (m²/g) ^b	Pore size (Å) ^b	Pore volume (cm³/g) ^b
1	GMC	5 wt% Mn/MgO	3.46	200	61.8	0.84
2		10 wt% Mn/MgO	3.44	190	62.1	0.81
3		15 wt% Mn/MgO	3.42	157	63.2	0.80
4	GMC (after calcination)	10 wt% Mn/MgO	—	103	63.7	0.80

^a The values calculated using XRD patterns.

^b The values obtained from N₂ adsorption-desorption studies.

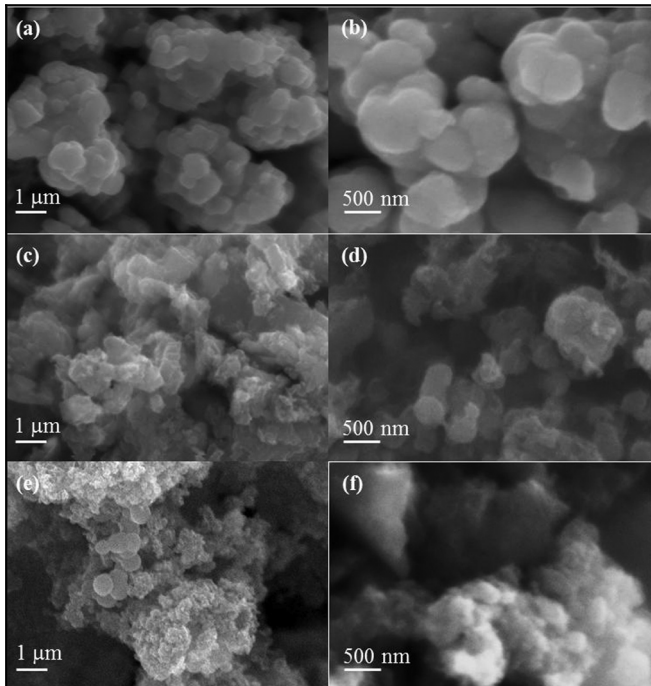


Fig. 5. SEM images of as-synthesized GMC with different magnification grown over the (a) & (b) 5 wt% Mn/MgO, (c) & (d) 10 wt% Mn/MgO and (e) & (f) 15 wt% Mn/MgO at 900 °C.

of GMC obtained over the 10 wt% Mn/MgO at different temperatures is shown in Fig. 7. The surface roughness increases with increasing the reaction temperature. The surface of GMC has little bigger pores obtained at 1000 °C when compared with other temperatures. This might be due to agglomeration of nanoparticles at high temperature, which after removing the metal particles makes a bigger pore. EDS measurement is used as a quantitative analysis for the presence of the oxygen and metal components on the surface of the mesoporous carbon. Carbon grosses the predominant part in the GMC with very trace amount of oxygen present, which is clearly seen in EDS spectrum. The oxygen content slightly increases with increase the reaction temperature which is clear from EDS image. Self-decomposition and oxidation might be occurring at high temperature, which can be responsible for the presence of increased oxygen content. Absence of catalytic templates and other impurities confirms the GMC is pure after acid treatments. This also ensures that the surface morphology of the GMC has not been damaged by the acid treatment.

Fig. 8 shows the TEM images of GMC with different magnifications obtained over the different wt% of Mn/MgO. The GMC produced using CVD method which contain impurities such as metal catalysts and amorphous carbons, normally make the detection of GMC impossible by TEM. After purification by acid treatment, the majority of impurities can be removed which leaves visible clear

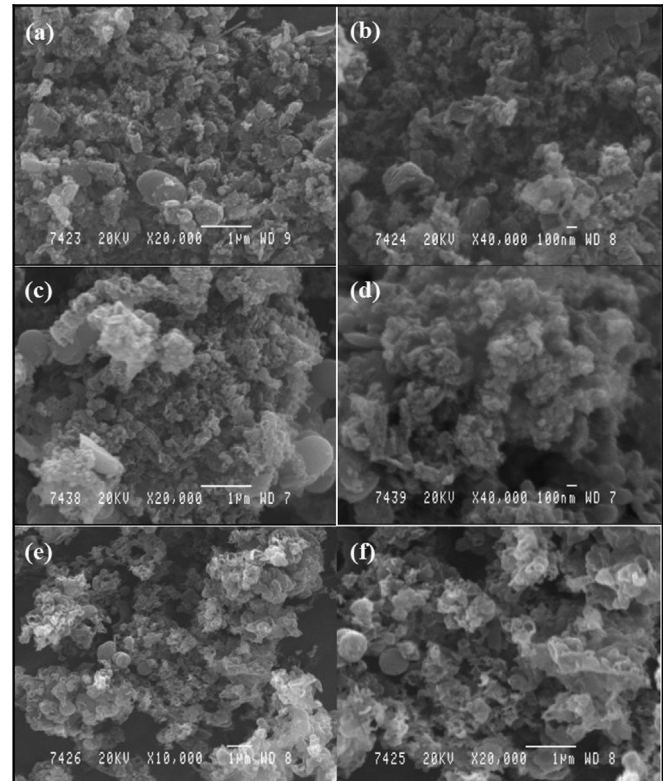


Fig. 6. SEM images of GMC with different magnification obtained over the (a) & (b) 5 wt% Mn/MgO, (c) & (d) 10 wt% Mn/MgO and (e) & (f) 15 wt% Mn/MgO at 900 °C.

GMC. The graphitic carbon obtained is cage like and exhibit a hollow core structure. Porous carbon combined over the graphitic carbon is clearly seen in TEM images [6]. The graphitic layer distance and layer thickness decreases with increasing the Mn concentration over the MgO support. Fig. 9 shows, the TEM images of GMC obtained over the 10 wt% Mn/MgO at different temperature from 800 to 1000 °C. The graphitization of GMC increased with increasing the reaction temperature up to 900 °C and then decreased. High porosity GMC with low degree of graphitization was obtained at 800 °C when compared to GMC prepared at 900 °C, which is clearly seen in Fig. 9. Further it was confirmed by nitrogen sorption analysis and Raman spectroscopy techniques. TEM images of GMC (after calcination) obtained over the 5wt% Mn/MgO, 10wt% Mn/MgO and 15wt% Mn/MgO which are shown in Figs. 10–12, respectively. The graphitization of GMC is clear from TEM images because during the calcinations majority of impurities such as amorphous carbon and most defected porous carbon is eliminated from host GMC materials. The graphitic layer thickness gradually decreases with increasing the metal concentration over the supported material and is clear with HRTEM images. Distance between the metal nanoparticles decreases with increasing the metal concentration. The graphitic carbon has grown over the metal nanoparticles so that the thickness of graphitic layer is low at high metal concentrations. As shown in Figs. 10(d), 11(d) and 12(d), the lattice fringes of the graphitic structure are clearly observed. This confirms that the prepared material is characteristic graphitic carbon with high degree of graphitization [30]. The interlayer distance is ~0.345–0.340 nm, which matches well with XRD results.

The graphitization of GMC not only depends on amount of metals particles over the catalytic support. Also the degree of graphitization depends on the reaction temperatures. So that the optimization of the reaction temperature is one of the factors for identify the excellent quality and quantity of GMC. Fig. 13 shows the

Table 2
Catalytic activities and reaction condition on the yield of GMC.

S. No	Synthesized material	Catalytic template	Yield of carbon deposition (%)		
			800 °C	900 °C	1000 °C
1	GMC	5 wt% Mn/MgO	—	670	—
2		10 wt% Mn/MgO	710	770	680
3		15 wt% Mn/MgO	—	760	—
4	GMC (after calcination)	10 wt% Mn/MgO	600	690	580

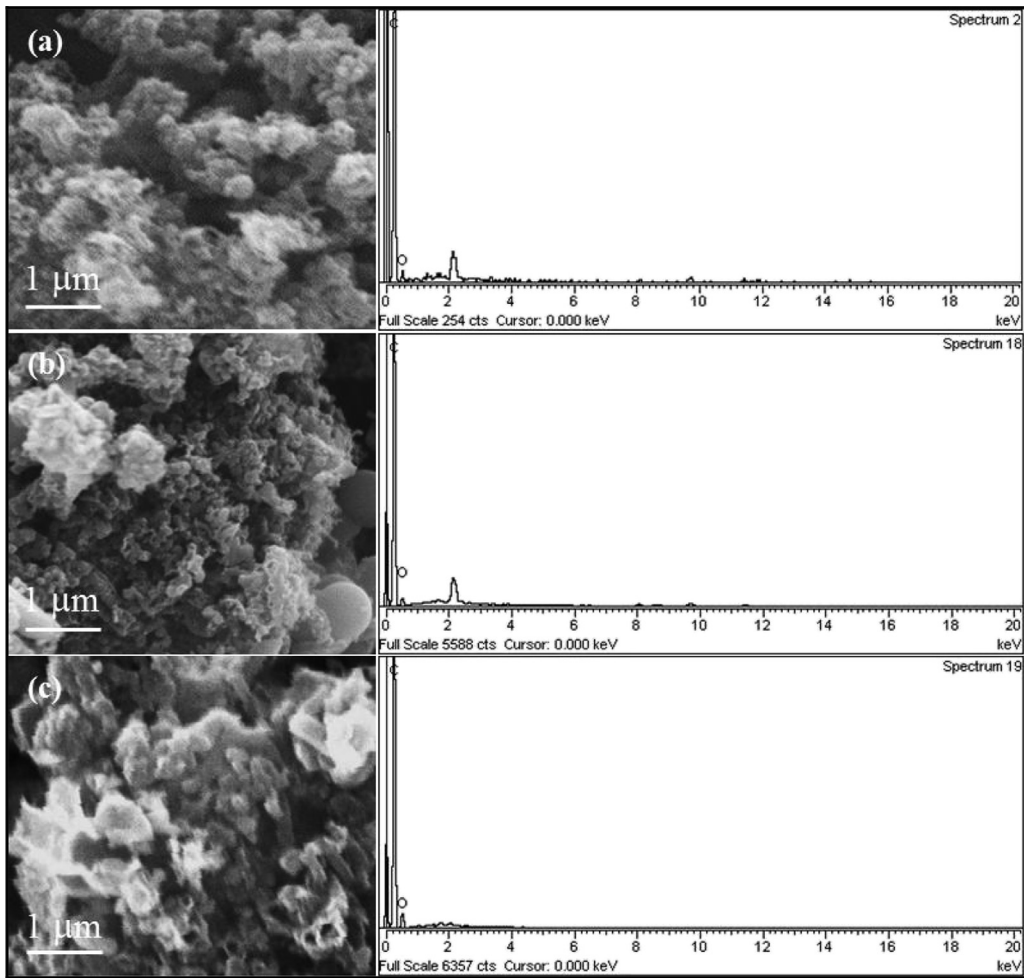


Fig. 7. SEM with EDS images of GMC obtained over the 10 wt% Mn/MgO at (a) 800 °C, (b) 900 °C and (c) 1000 °C.

TEM images of GMC (after calcination) obtained over the 10 wt% Mn/MgO at different temperatures from 800 to 1000 °C. The prepared GMC is nearly similar at 800 and 900 °C but has bigger graphitic hole at 1000 °C. The metal particles agglomeration and cluster formation is possible at high temperature. The carbon deposition over the agglomerated nanoparticles results in bigger graphitic carbon. After removal of metal particles by the acid treatment and amorphous carbon by calcinations, bigger pores of GMC are visible. Graphitizable carbon with an ordered porosity is clear from HR-TEM images. The GMC wall thickness appears around 0.34 nm without major defect. So the arrays of the constructed GMC might have high mechanical strength when compared with commercial GMC. Generally, GMC prepared from acetylene (C_2H_2) often suffer from amorphous carbon coating due to their self-pyrolysis at elevated temperature. But the present work deals with the synthesized hollow core structured and graphitized mesoporous carbon without major contaminations using Mn/MgO as a catalytic template and C_2H_2 as a carbon source, by the CVD method at different temperatures. SEM and TEM techniques are used to characterize the morphology of the GMC and to ensure that the structure of the GMC has not been destroyed by the acid treatment and calcination.

3.5. Raman spectroscopy studies of GMC

Raman spectroscopy is one of the most powerful tools for characterization of graphite related carbon materials. Raman

spectra of GMC obtained over the different wt% of Mn/MgO at 900 °C are shown in Fig. 14. The spectra shows the two major peaks at 1600 cm^{-1} and 1350 cm^{-1} , which correspond to G-band (graphite band) and D-band (disorder band), respectively. The D-band is often attributed to disordered scattering, which results from the imperfection or loss of hexagonal symmetry of the graphite structure. The G-band observed at 1600 cm^{-1} has been assigned to the Raman-allowed phonon E_{2g} (stretching) mode of graphite. The strongest peak of G-band in the spectrum indicates the formation of good arrangement of hexagonal lattice of graphite [31]. The band at 1350 cm^{-1} corresponds to the D-band and assigned to the A_{1g} phonon is weak which reveals the high purity of the synthesized GMC. The relative intensity ratio of the D band vs the G band (I_D/I_G) for GMC is less than 1, indicating that GMC is composed of small graphene sheets with a high degree of graphitization [15,32,33]. The degree of graphitization increased with increasing the metal concentration over the support then decreased. The number of graphene sheets decreased with increased the metal concentration over the MgO catalytic support due to insufficient space for the growth of GMC in specific area. The degree of graphitization depends on perfect arrangement (well ordering) of graphene sheets not depending on thickness of graphene bunch. The graphitic layer has more disorder in graphene bunch, which has low degree of graphitization. The optimum of metal concentration is around 10 wt% Mn/MgO for the better formation of GMC. The reason behind the graphitization has been discussed in the previous section. The relative intensity ratio of D

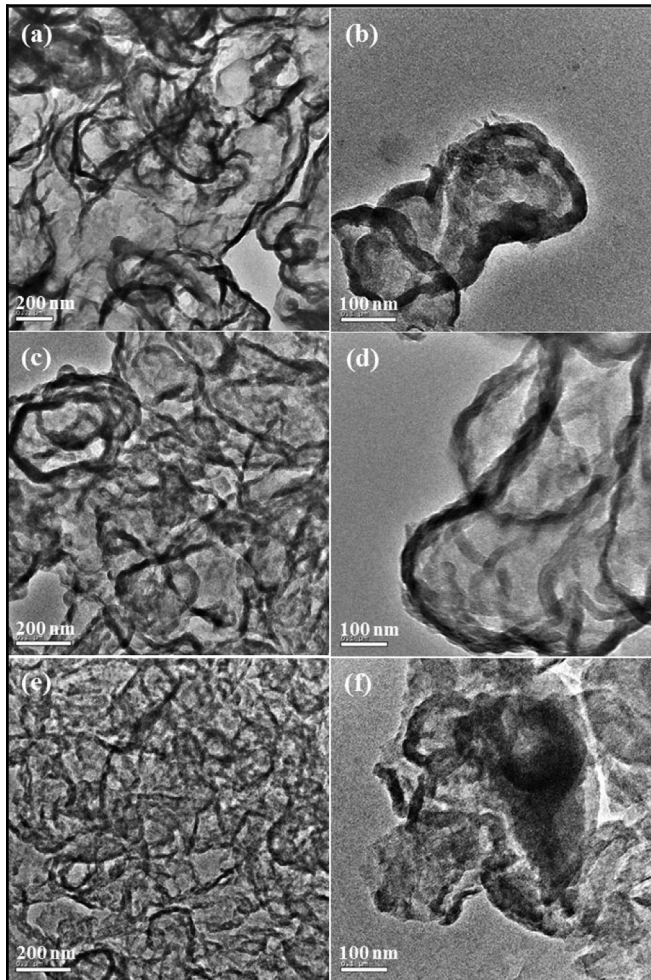


Fig. 8. TEM images of GMC with different magnification obtained over the (a) & (b) 5 wt% Mn/MgO, (c) & (d) 10 wt% Mn/MgO and (e) & (f) 15 wt% Mn/MgO at 900 °C.

band to the G band for GMC obtained over the 10 wt% Mn/MgO is 0.79. The optimum wt% was examined by different temperatures for the maximum yield and high degree of graphitization. Fig. 15 depicts the spectra of GMC obtained over the 10 wt% Mn/MgO at different temperatures from 800 to 1000 °C. The temperature study confirmed that the reaction at 900 °C is optimum temperature for the production of GMC with high degree of graphitization compared to the other temperatures. In general, highly graphitic carbon materials combined with amorphous carbon/disordered carbon have shown low degree of graphitization in Raman spectrum. Amorphous carbon/disordered carbon can be easily removed

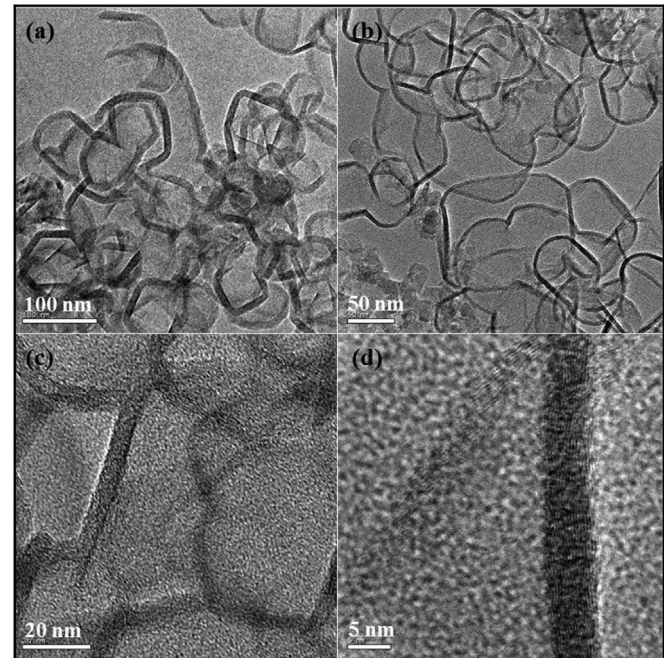


Fig. 10. TEM images of GMC (after calcination) with different magnification obtained over 5 wt% Mn/MgO at 900 °C.

from the graphitic materials by calcination. Raman spectra of GMC (after calcination) obtained over the 10 wt% Mn/MgO at different temperatures from 800 to 1000 °C are shown in Fig. 16. After calcination, the degree of graphitization increased considerably which is clear from the spectra for all samples. The I_D/I_G ratios before calcination were ca. 0.93, 0.79, and 0.98 at 800, 900, and 1000 °C, respectively, which after calcination were ca. 0.73, 0.61, and 0.80, respectively. The degree of graphitization increased and surface area decreased after calcination, which is due to elimination of amorphous carbon/defected porous carbon from the host GMC.

3.6. Catalytic activities, reaction mechanism and yield of GMC

Generally, the transition metal containing mesoporous materials (silica based materials/metal oxides) are used as catalytic template for the preparation of mesoporous carbon with graphitization. Because these types of materials have large surface area, large pore volume, narrow pore size distribution, and easy surface functionalization. Metal nanoparticle is seed for the production of graphitic carbon materials such fullerenes, CNTs, and graphitic carbon using acetylene as a carbon precursor by the CVD method. In this article, we have used metal impregnated MgO (light) as a

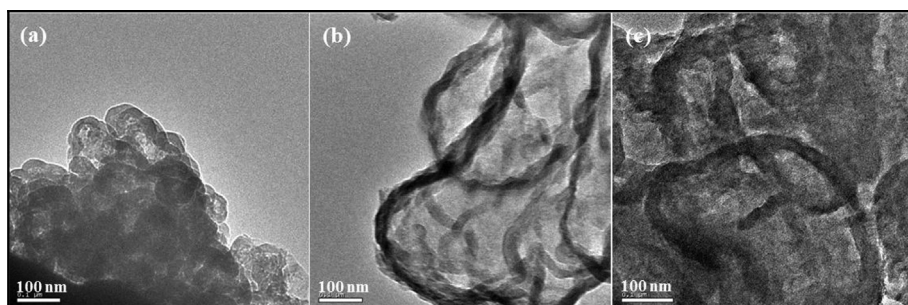


Fig. 9. TEM images of GMC obtained over the 10 wt% Mn/MgO at (a) 800 °C, (b) 900 °C and (c) 1000 °C.

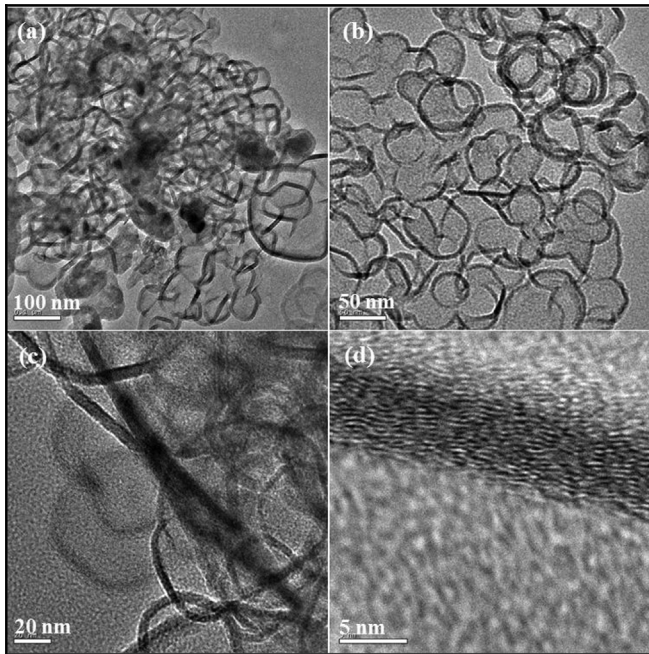


Fig. 11. TEM images of GMC (after calcination) with different magnification obtained over 10 wt% Mn/MgO at 900 °C.

catalytic template and acetylene as a carbon precursor for the production of GMC by CVD method. MgO is a thermally stable and lightweight material. Already, metal containing MgO has used for the preparation of CNTs and carbon related nanostructured materials. The reaction carried out without Mn metal particles; the carbon deposition was very low. So that we concluded that, the reaction activity depends on the concentration of Mn particles over the MgO catalytic templates. Our work Mn is seed for the growth of GMC. Further, the reaction temperatures and metal concentrations

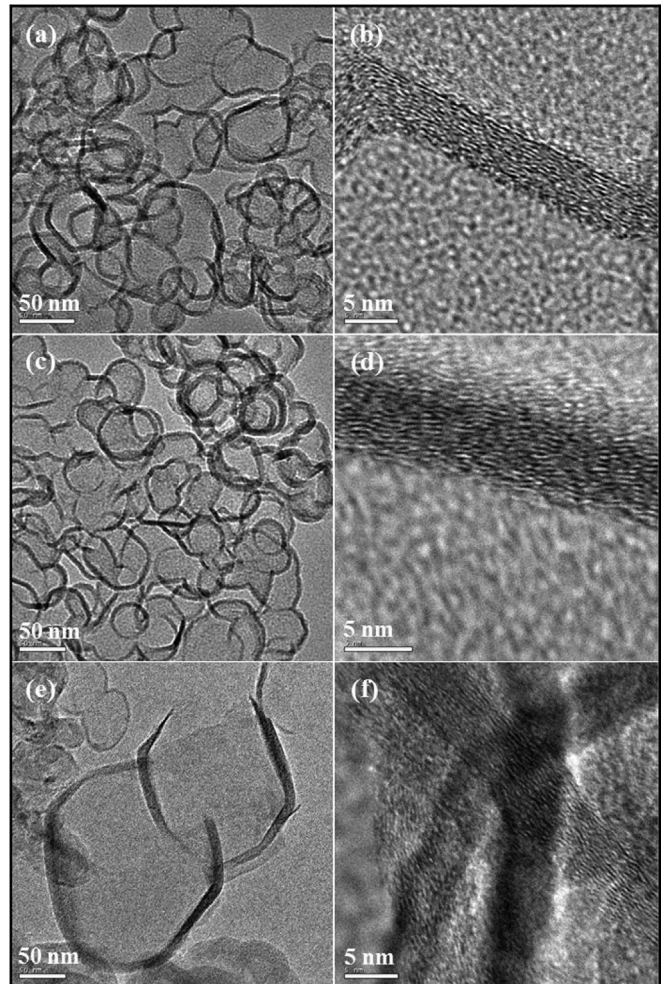


Fig. 13. TEM images of GMC (after calcination) with different magnification obtained over 10 wt% Mn/MgO at (a) & (b) 800 °C, (c) & (d) 900 °C and (e) & (f) 1000 °C.

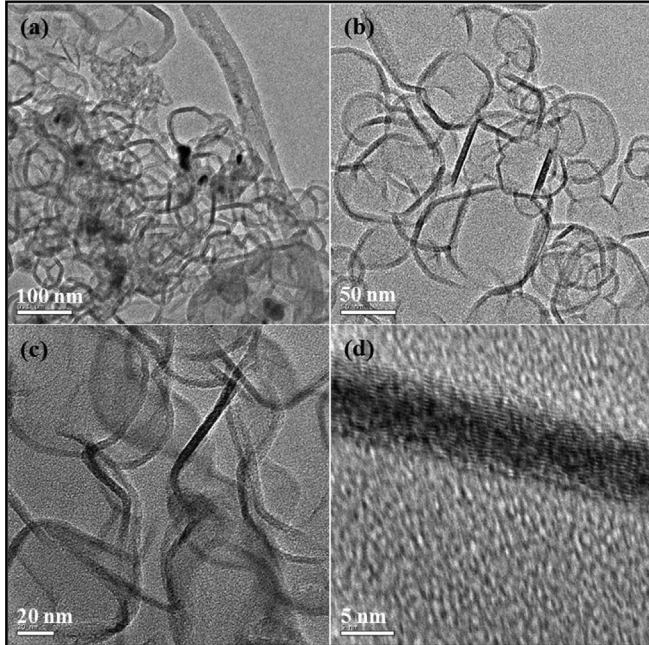


Fig. 12. TEM images of GMC (after calcination) with different magnification obtained over 15 wt% Mn/MgO at 900 °C.

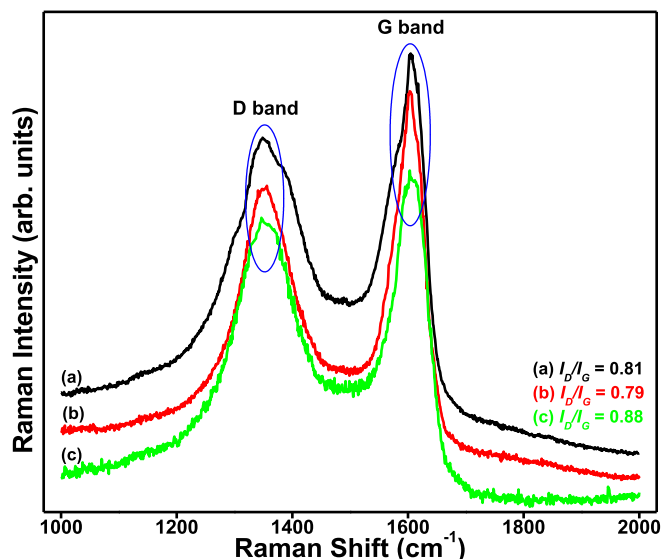


Fig. 14. Raman spectrum of GMC obtained over the (a) 5 wt% Mn/MgO (b) 10 wt% Mn/MgO and (c) 15 wt% Mn/MgO at 900 °C.

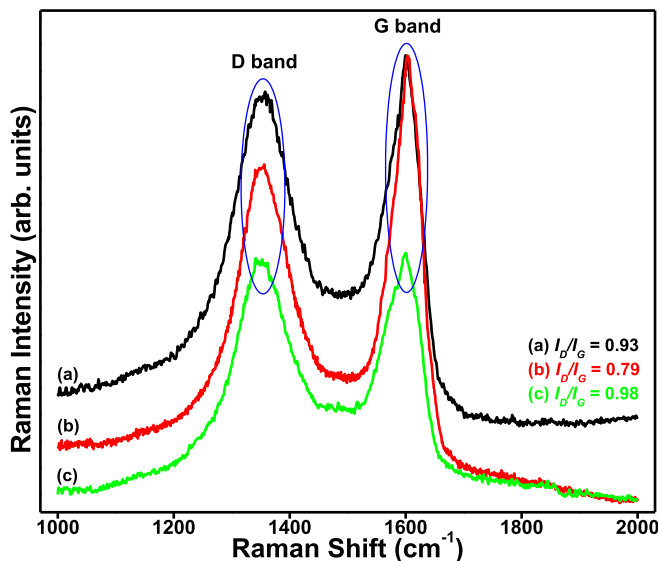


Fig. 15. Raman spectrum of GMC obtained over the 10 wt% Mn/MgO at (a) 800 °C (b) 900 °C and (c) 1000 °C.

over the MgO support were optimized for the better production of GMC with high yield. The acetylene gas decomposed to carbon and formed graphene layer over the metal nanoparticles. The yield of carbon depends on the metal concentration over the support. The carbon deposition increased with increasing the metal concentration beyond the optimum level, the yield of carbon deposition decreased due to hindrance of space for the growth of carbon material. From the acetylene decomposition, the deposited carbon materials and their catalytic activity depending on the wt% of Mn over the MgO support were found to be in the decreasing order as follows: 10 wt% Mn/MgO > 5 wt% Mn/MgO > 15 wt% Mn/MgO. 10 wt% Mn/MgO offered a larger amount of carbon deposition when compared with the other Mn/MgO ratios at 900 °C. After deposition the catalytic template was removed from synthesized porous carbon materials by acid treatment which results in the formation of pores in the GMC. The graphitization and yield of GMC have already discussed in previous sections.

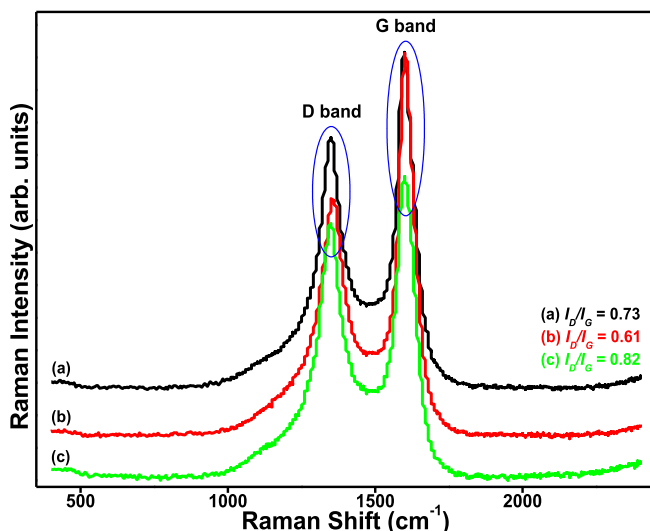


Fig. 16. Raman spectrum of GMC (after calcination) obtained over the 10 wt% Mn/MgO at (a) 800 °C (b) 900 °C and (c) 1000 °C.

The yield of GMC increased with increasing the reaction temperature and the optimum of reaction temperature has found to be around 900 °C. Further increase in temperature leads to the decrease in yield. From the acetylene decomposition, the 10 wt% Mn/MgO catalytic template in terms of synthesis yield of GMC at different temperatures follows the order of 900 °C > 800 °C > 1000 °C. The reaction temperature 900 °C offered larger amount of carbon deposition over the 10 wt% Mn/MgO when compared with the other reaction temperatures. From the experimental results it is observed that the metal concentration over the support and the reaction temperature also play a potential role for the synthesis of GMC by CVD method. The yield of GMC using different wt% of catalytic templates and reaction temperature are summarized in Table 2. The GMC obtained over Mn/MgO possesses highly graphitic and mesoporous which might be useful to enhance electronic and thermomechanical properties. So Mn/MgO assisted CVD, depicted as an ideal choice for the production of GMC with high graphitization.

The purification is one of the factors to decide the purity of the final products. The synthesized GMC contain catalytic templates, which normally make more complex for the detection of GMC and leads to the limited application. For example, if we use porous silica as a catalytic templates for the production of GMC. The removal of silica from the mesoporous carbon is difficult. In this case, we have to use strong hydrofluoric acid for the removal of silica from host GMC and during the purification process the ordered structure of GMC will be damaged. Moreover, the hydrofluoric acid is a highly corrosive and is a contact poison when compared with HCl and HNO₃. The MgO catalytic template removed easily from host GMC by dilute mixture of HCl and HNO₃ treatment. The MgO catalytic template is easily available and very cheap. To the best of our knowledge, this is the first instance we produced GMC over the Mn/MgO catalytic templates using acetylene as a carbon precursor by CVD method.

4. Conclusions

In the present study, first instant of mesoporous carbon with graphitic order was synthesized using decomposition of acetylene over the Mn/MgO catalytic template at 900 °C by the CVD method. Raman I_D/I_G value of GMC showed the high degree of graphitization. The XRD pattern also supports the formation of GMC is high purity with well graphitized. Mn/MgO is very cheap and can be removed easily using dilute mixture of HCl and HNO₃ instead of the corrosive HF. This method of synthesis is very simple and effective because of the moderate temperature used and the cost also effectiveness for mass production. The prepared GMC might be an ideal candidate for the electronics and thermomechanical applications.

Acknowledgment

This work was supported by Priority Research Centers Program through the National Research Foundation of Korea (NRF) funded by the Ministry of Education (2014R1A6A1031189).

References

- [1] Y. Wang, M. Yao, Y. Chen, Y. Zuo, X. Zhang, L. Cui, *J. Alloy. Compd.* 627 (2015) 7–12.
- [2] S. Liu, S. Li, H. Niu, T. Zeng, Y. Cai, C. Shi, B. Zhou, F. Wu, X. Zhao, *Micropor. Mesopor. Mater.* 200 (2014) 151–158.
- [3] D.S. Cameron, S.J. Cooper, I.L. Dodgson, B. Harrison, J.W. Jenkins, *Catal. Today* 7 (1990) 113–137.
- [4] S.H. Chai, J.Y. Howe, X. Wang, M. Kidder, V. Schwartz, M.L. Golden, S.H. Overbury, S. Dai, D.E. Jiang, *Carbon* 50 (2012) 1574–1582.
- [5] K. Xiong, Y. Zhang, J. Lia, K. Liew, *J. Energy Chem.* 22 (2013) 560–566.
- [6] J. Qi, L. Jiang, S. Wang, G. Sun, *Appl. Catal. B Environ.* 107 (2011) 95–103.

- [7] S. Numao, K. Judai, J. Nishijo, K. Mizuuchi, N. Nishi, *Carbon* 47 (2009) 306–312.
- [8] Y. Dong, H. Lin, D. Zhou, H. Niu, Q. Jin, F. Qu, *Electrochim. Acta* 159 (2015) 116–123.
- [9] F. Wang, L. Liang, L. Shi, M. Liu, J. Sun, *J. Alloy, Compound* 633 (2015) 65–70.
- [10] P. Li, Y. Liu, J. Liu, Z. Li, G. Wu, M. Wu, *Chem. Eng. J.* 271 (2015) 173–179.
- [11] C. Liang, Z. Li, S. Dai, *Angew. Chem. Int. Ed.* 47 (2008) 3696–3717.
- [12] R. Atchudana, A. Pandurangan, J. Joo, *Micropor. Mesopor. Mater.* 175 (2013) 161–169.
- [13] K.L. Choy, *Prog. Mater. Sci.* 48 (2003) 57–170.
- [14] K. Koziol, B.O. Boskovic, N. Yahya, in: N. Yahya (Ed.), *Carbon and Oxide Nanostructures, Adv. Struct. Mater.*, vol. 5, Springer-Verlag, Berlin Heidelberg, 2010.
- [15] D. Yuan, X. Yuan, W. Zou, F. Zeng, X. Huang, S. Zhou, *J. Mater. Chem.* 22 (2012) 17820–17826.
- [16] G. Yang, H. Han, T. Li, C. Du, *Carbon* 50 (2012) 3753–3765.
- [17] Y. Seo, K. Kim, Y. Jung, R. Ryoo, *Micropor. Mesopor. Mater.* 207 (2015) 156–162.
- [18] R. Atchudan, A. Pandurangan, K. Subramanian, *Appl. Surf. Sci.* 258 (2011) 1045–1051.
- [19] R. Atchudan, A. Pandurangan, J. Joo, *J. Nanosci. Nanotechnol.* 15 (2015) 4255–4267.
- [20] T. Suzuki, S. Inoue, Y. Ando, *Diam. Relat. Mater.* 17 (2008) 1596–1599.
- [21] R. Atchudan, A. Pandurangan, *J. Mol. Catal. A Chem.* 355 (2012) 75–84.
- [22] S. Azzaza, M. El-Hilo, S. Narayanan, J. Judith Vijaya, N. Mamouni, A. Benyoussef, A. El Kenz, M. Bououdin, *Mater. Chem. Phys.* 143 (2014) 1500–1507.
- [23] J.C. Juan, Y. Jiang, X. Meng, W. Cao, M.A. Yarmo, J.C. Zhang, *Mater. Res. Bull.* 42 (2007) 1278–1285.
- [24] D. Zhai, H. Du, B. Li, Y. Zhu, F. Kang, *Carbon* 49 (2011) 718–736.
- [25] M. Sevilla, C. Sanchis, T. Valdés-Solís, E. Morallón, A.B. Fuertes, *J. Phys. Chem. C* 111 (2007) 9749–9756.
- [26] J. Qi, L. Jiang, Q. Tang, S. Zhu, S. Wang, B. Yi, G. Sun, *Carbon* 50 (2012) 2824–2831.
- [27] W. Li, D. Chen, Z. Li, Y. Shi, Y. Wan, J.G. Wang, Z. Jiang, D. Zhao, *Carbon* 45 (2007) 1757–1763.
- [28] B. Xu, L. Peng, G. Wang, G. Cao, F. Wu, *Carbon* 48 (2010) 2361–2380.
- [29] Y. Jung, H.I. Lee, J.H. Kim, M.H. Yun, J. Hwang, D.H. Ahn, J.N. Park, J.H. Boo, K.S. Choi, J.M. Kim, *J. Mater. Chem.* 20 (2010) 4663–4668.
- [30] Z. Fu-long, Y. Xiao-li, Z. Wu-jun, H. Xiang-jin, M. Shan-shan, Y. Ding-sheng, *New Carbon Mater.* 28 (2013) 121–126.
- [31] M. Wu, P. Ai, M. Tan, B. Jiang, Y. Li, J. Zheng, W. Wu, Z. Li, Q. Zhang, X. He, *Chem. Eng. J.* 245 (2014) 166–172.
- [32] R. Atchudan, A. Pandurangan, *Micropor. Mesopor. Mater.* 167 (2013) 162–175.
- [33] Q. Yang, W. Xu, A. Tomita, T. Kyotani, *Chem. Mater.* 17 (2005) 2940–2945.